Inorg. Chem. **2007**, *46*, 7960–7970

Highly Selective Ferric Ion Sorption and Exchange by Crystalline Metal Phosphonates Constructed from Tetraphosphonic Acids

Jie Wu, Hongwei Hou,* Huayun Han, and Yaoting Fan

Department of Chemistry, Zhengzhou University, Henan 450052, People's Republic of China

Received October 19, 2006

With the motivation of searching for highly selective ferric ion sorbents, two open-framework and microporous materials, $\{[Pb_7(HEDTP)_2(H_2O)]\cdot 7H_2O\}_n$ (**1**) and $\{[Zn_2(H_4EDTP)]\cdot 2H_2O\}_n$ (**2**) [H_8EDTP = *N*,*N*,*N*′,*N*′-ethylenediaminetetrakis(methylenephosphonic acid)], have been synthesized and structurally characterized. The structure of compound **1** results from the seven crystallographically different lead atoms that are bridged by two $HEDTP^{7-}$ ligands to yield a three-dimensional microporous framework with tunnels along the *a* and *b* axes. Compound **2** features a layer architecture built of square waves along the *a* axis. The layers are connected by hydrogen bonds between uncoordinated phosphonate oxygen atoms to form a three-dimensional supramolecular network, with one-dimensional tunnels along the *a* axis. Both compounds **1** and **2** exhibited high ion sorption and exchange capacities for millimolar concentrations of Fe^{III}. Specifically, when 0.01 g of **1** (or **2**) was added to 5 mL of a 1 mM metallic chloride aqueous solution and the mixture was allowed to stand for 2 days at room temperature, compound **1** adsorbed nearly 100% of Fe^{III} and compound **2** adsorbed 96.8% of Fe^{III}. They were also found to adsorb ferric ions selectively over other metal ions, such as Ca^{II}, Cr^{II}, Mn^{II}, Cu^{II}, Zn^{II}, Cd^{II}, etc. Their special ferric ion uptake capacities may be attributed to the cation exchange, coordination bonding, and electrostatic attraction between ferric ions and metal phosphonates.

Introduction

The selective uptake of ferric ions from aqueous solutions is exceedingly important because of its significant role in the areas of environment, medicine, and biology, as well as its wide application in proton conductivity and an ion-exchanger-supported iron-containing catalyst.[1] Especially in clinical medicine, thalassemias and genetic hemochromatosis are ferric ion overload diseases, which can be effectively treated by iron chelation therapy to remove ferric ions.[2] However, natural and synthetic clinical iron chelators could affect biological processes involving iron and other metal ions in health and disease states.[3] This problem underlines the current efforts for developing effective ion sorption and exchange materials with high selectivity for ferric ions versus other common metal ions present in biological systems. Then, how can we achieve such materials?

In a sense, the research for the micro- and mesoporous materials as ion sorbents and exchangers is derived from zeolites, which are the representative examples.[4] Zeolites have a large pore volume that is usually occupied by various cations and water molecules. The entrapped cations and water molecules can be replaced by certain salts, depending upon the types of zeolites.[5] However, the limitations of zeolites are that their tunnel and pore sizes are no large than about 10 Å and they are unstable toward acid solutions.[6] A new

* To whom correspondence should be addressed. E-mail: houhongw@zzu.edu.cn. Tel and Fax: +86-371-67761744.

(1) (a) Jonathan, B.; Kiyoshi, M. *Nature* **2004**, *432*, 811. (b) Shiota, Y.; Suzuki, K.; Yoshizawa, K. *Organometallics* **2006**, *25*, 3118. (c) Webb, J.; Macey, D. J.; Chua-anusorn, W.; Pierre, T. G. St.; Brooker, L. R.; Rahman, I.; Noller, B. *Coord. Chem. Rev.* **1999**, *190*−*192*, 1199. (d) Kawabata, T.; Ohishi, Y.; Itsuki, S.; Fujisaki, N.; Shishido, T.; Takaki, K.; Zhang, Q.-H.; Wang, Y.; Takehira, K. *J. Mol. Catal. A* **2005**, *236*, 99. (e) Clearfield, A. In *New Developments in Ion Exchange Materials*; Abe, M., Kataoka, T., Suzuki, T., Eds.; Kodansha, Ltd.: Tokyo, 1991.

(2) (a) Chaim, H.; Gabriela, L.; Abraham, M. K.; Loav, C. Z. *Ann. N. Y. Acad. Sci.* **2005**, *1045*, 124. (b) Wang, C.-H.; Wu, K.-H.; Tsai, F.-J.; Peng, C.-T.; Tsai, C.-H. *Hemoglobin* **2006**, *30*, 257.

(3) Nathan, D. G. *Ann. N. Y. Acad. Sci.* **2005**, *1054*, 1.

(4) (a) Breck, D. W. *Zeolite Molecular Sieves*; Wiley: New York, 1974; p 498. (b) Watanabe, Y.; Yamada, H.; Kokusen, H.; Tanaka, J.; Moriyoshi, Y.; Komatsu, Y. *Sep. Sci. Technol.* **2003**, *38*, 1519.

(5) Földesová, M.; Dillinger, P.; Lukác, P. *J. Radioanal. Nucl. Chem.* **1999**, *242*, 227.

(6) Subbiah, A.; Pyle, D.; Rowland, A.; Huang, J.; Narayanan, R. A.; Thiyagarajan, P.; Zoń, J.; Clearfield, A. *J. Am. Chem. Soc.* **2005**, *127*, 10826.

10.1021/ic062014x CCC: $37.00
Published on Web 08/16/2007

direction applied to the research was to synthesize hydrous metal oxides[7] and organic resins[8] as ion sorbents and exchangers, which soon dominated the field. Nevertheless, organic-based ion sorbents and exchangers face thermal stability challenges. Some metal−organic compounds with open frameworks, such as metal phosphonates[9] and chalcogenides,[10] have been considered as excellent ion sorbents and exchangers afterward because of their greater chemical, compositional, and structural diversity, as well as their high resistance toward temperature and radiation. For example, Clearfield et al. have reported zirconium phosphate−phosphonates, which have been successfully used in intercalation host, ionic conductivity, and ion sorption and exchange.[9] These metal phosphonates are a class of ion-exchange sorbents that possess effective ion-exchange capacity and are more thermally stable than the commonly used organic-based exchangers.[11] More importantly, the selectivity of metal phosphonate for polyvalent cations is very high, and analytical separation or concentration of these cations can be performed.[12] Therefore, our interest is focused on employing tetraphosphonic acids $\{(H_2O_3PCH_2)_2N-R-N(CH_2PO_3H_2)_2$ [R = $(CH_2)_2$, $(CH_2)_4$, C_6H_4, etc.]} as polytopic organic building blocks to yield metal tetraphosphonates with novel open-framework and microporous structures.[13] These metal tetraphosphonates as stable organic−inorganic hybrid materials display both microporous structures and metal phosphonate properties in conjunction with robust inorganic backbones, thus having potential applications in selective ion sorption and exchange. By the right choice of the interlinking organic group, we can modify and tailor the dimensions of the tunnels inside these structures to suit certain ions, such as Fe^{III}.

Herein we used a tetraphosphonic acid, $[(H_2O_3PCH_2)_2N(CH_2)_2N(CH_2PO_3H_2)_2]$ (H_8EDTP), to prepare two novel divalent metal tetraphosphonates, namely, $\{[Pb_7(HEDTP)_2(H_2O)]\cdot 7H_2O\}_n$ (**1**), whose structure features a three-dimensional microporous network with tunnels along the *a* and *b* axes, and $\{[Zn_2(H_4EDTP)]\cdot 2H_2O\}_n$ (**2**), whose structure contains square-wave-like layers interconnected by hydrogen bonds to form a three-dimensional supramolecular network, with one-dimensional tunnels along the *a* axis. Both compounds show highly selective cation sorption and exchange capacities for Fe^{III} ions versus other metal ions and become promising candidates for effective clinical iron chelators. We think the selective ferric ion sorption of such compounds may arise not only from ion exchange but also from the strong coordination bonding and electrostatic attractions to ferric ions with phosphonate groups.

Experimental Section

N,*N*,*N*′,*N*′-Ethylenediaminetetrakis(methylenephosphonic acid) (H_8EDTP) was synthesized according to the literature.[14] All other starting materials were of reagent quality and were obtained from commercial sources without further purification. IR data were recorded on a Nicolet NEXUS 470-FTIR spectrophotometer with KBr pellets in the 400−4000 cm^{-1} region. Elemental analyses (C, H, and N) were carried out on a FLASH EA 1112 analyzer. Atom adsorption analysis was conducted on a Hitch Z-8000 atom adsorption analyzer. Measurements of the pH values were carried out on a pH meter of model 6071 (Jenco Electronics, Ltd., Shanghai, China). The surface area was measured by using Quantanchrome NOVA 1000e with N_2. Powder X-ray diffraction (XRD) patterns were recorded using Cu $K\alpha_1$ radiation on a PANalytical X'prtPro diffractometer. Field emission scanning electron microscopy (SEM) and energy-dispersive X-ray spectrometry (EDS) were conducted on a JEOL JSM-6700F scanning electron microscope.

Preparation of $\{[Pb_7(HEDTP)_2(H_2O)]\cdot 7H_2O\}_n$ (1). A mixture of lead(II) acetate (3 mmol), LiF (1 mmol), and H_8EDTP (1 mmol) in 8 mL of distilled water and 2 mL of C_2H_5OH, adjusted to pH 5−6 with $N(CH_2CH_3)_3$, was kept in a Teflon-lined autoclave at 140 °C for 4 days. After slow cooling to room temperature, colorless blocky crystals were obtained together with a white powder. The colorless crystals were manually collected and were further used for single-crystal analysis and physical measurements. Yield: 35% based on Pb. Anal. Calcd for $C_{12}H_{40}N_4O_{32}P_8Pb_7$: C, 5.88; H, 0.98; N, 2.29. Found: C, 5.94; H, 1.09; N, 2.17. IR (KBr, cm^{-1}): 3423(w), 3131(w), 2342(w), 1628(s), 1400(s), 1064(w), 974(w), 781(w), 571(w).

Preparation of $\{[Zn_2(H_4EDTP)]\cdot 2H_2O\}_n$ (2). The hydrothermal treatment of a mixture of $ZnCl_2$ (1 mmol), LiF (1 mmol), H_8EDTP (1 mmol), distilled water (5 mL), and C_2H_5OH (5 mL), adjusted by $N(CH_2CH_3)_3$ to pH 5.3, in a Teflon-lined autoclave at 160 °C for 4 days, resulted in the formation of the colorless block crystals of compound **2** as a monophasic material. Yield: 77% based on Zn. Anal. Calcd for $C_6H_{22}N_2O_{14}P_4Zn_2$: C, 11.98; H, 3.66; N, 4.66; Found: C, 12.17; H, 3.54; N, 4.19. IR (KBr, cm^{-1}): 3424(w), 3001(w), 2775(w), 1640(s), 1447(s), 1143(s), 1001(w), 935(w), 762(w), 559(w).

Crystallographic Studies. Single crystals of dimensions 0.26 × 0.13 × 0.10 mm^3 for **1** and 0.11 × 0.10 × 0.06 mm^3 for **2** were selected for indexing and intensity data collection on a Bruker

(7) (a) Subramanian, M. A.; Aravamudan, G.; Subba Rao, G. V. *Prog. Solid State Chem.* **1983**, *15*, 55. (b) Machida, M.; Miyazaki, K.; Matsushima, S,; Arai, M. *J. Mater. Chem.* **2003**, *13*, 1433.
(8) (a) Kavallieratos, K.; Rosenberg, J. M.; Chen, W.-Z.; Ren, T. *J. Am. Chem. Soc.* **2005**, *127*, 6514. (b) Kavallieratos, K.; Rosenberg, J. M.; Bryan J. C. *Inorg. Chem.* **2005**, *44*, 2573. (c) Yordanov, A. T.; Roundhill, D. M. *Coord. Chem. Rev.* **1998**, *170*, 93.
(9) (a) Clearfield, A.; Duax, W. L.; Medina, A. S.; Smith, G. D.; Thomas, J. R. *J. Phys. Chem.* **1969**, *78*, 3424. (b) Sharma, C. V. K.; Chusuei, C. C.; Cléarc, R.; Möller, T.; Dunber, K. R.; Clearfield, A. *Inorg. Chem.* **2003**, *42*, 8300. (c) Kong, D.-Y.; Medvedev, D. G.; Clearfield, A. *Inorg. Chem.* **2004**, *43*, 7308. (d) Clearfield, A.; Sharma, C. V. K.; Zhang, B.-L. *Chem. Mater.* **2001**, *13*, 3099.
(10) (a) Manos, M. J.; Iyer, R. G.; Quarez, E.; Liao, J. H.; Kanatzidis, M. G. *Angew. Chem., Int. Ed.* **2005**, *44*, 3552. (b) Ding, N.; Kanatzidis, M. G. *Angew. Chem., Int. Ed.* **2006**, *45*, 1397. (c) Ding, N.; Chung, D.-Y.; Kanatzidis, M. G. *Chem. Commun.* **2004**, 1170.
(11) (a) Clearfield, A. *Chem. Rev.* **1988**, *88*, 125. (b) Yantasee, W.; Lin, Y.-H.; Fryxell, G. E.; Busche, B. J.; Birnbaum, J. C. *Sep. Sci. Technol.* **2003**, *38*, 3809. (c) Clearfield, A. Metal phosphonate chemistry. In *Progress in Inorganic Chemistry*; Karlin, K. D., Ed.; John Wiely & Sons: New York, 1998; Vol. 47, pp 371−510 and references cited therein. (d) Maeda, K. *Microporous Mesoporous Mater.* **2004**, *73*, 47. (e) Wang, J. D.; Clearfield, A.; Peng, G.-Z. *Mater. Chem. Phys.* **1993**, *35*, 208.
(12) Alberti, G. *Acc. Chem. Res.* **1978**, *11*, 163.
(13) (a) Vasylyev, M.; Neumann, R. *Chem. Mater.* **2006**, *18*, 2781. (b) Stock, N.; Guillou, N.; Senker, J.; Férey, G.; Bein, T. *Z. Anorg. Allg. Chem.* **2005**, *631*, *575*. (c) Demadis, K. D.; Mantzaridis, C.; Raptis, R. G.; Mezei, G. *Inorg. Chem.* **2005**, *44*, 4469. (d) Stock, N.; Stoll, A.; Bein, T. *Microporous Mesoporous Mater.* **2004**, *69*, 65. (e) Stock, N.; Bein, T. *Angew. Chem., Int. Ed.* **2004**, *43*, 749. (f) Vivani, R.; Costantino, F.; Costantino, U.; Nocchetti, M. *Inorg. Chem.* **2006**, *45*, 2388. (g) Stock, N.; Rauscher, M.; Bein, T. *J. Solid State Chem.* **2004**, *177*, 642.
(14) Princz, E.; Szilágyi, I.; Mogyorósi, K.; Labádi, I. *J. Therm. Anal. Calorim.* **2002**, *69*, 427.

Table 1. Crystallographic Data for Compounds **1** and **2**

compound	**1**	**2**
formula	$C_{12}H_{40}N_4O_{32}P_8Pb_7$	$C_6H_{20}N_2O_{14}P_4Zn_2$
fw	2450.57	598.86
space group	*P*2(1)/*n*	*Pca*2(1)
a/Å	14.9965(10)	8.2607(6)
b/Å	10.6476(7)	13.0802(9)
c/Å	28.1197(19)	16.9503(12)
α/deg	90.00	90
β/deg	104.8130(10)	90
γ/deg	90.00	90
V/Å^3	4340.8(5)	1831.5(2)
Z	4	4
ρ_{calc}/(Mg/m^3)	3.750	2.172
T/K	273(2)	273(2)
λ(Mo Kα)/Å	0.71073	0.71073
final R1,[a] wR2[b]	0.0447, 0.1131	0.0271, 0.0649
R indices (all data)	0.0554, 0.1187	0.0338, 0.0686

[a] $R1 = \sum||F_o| - |F_c||/\sum|F_o|$. [b] $wR2 = [\sum w(|F_o^2| - |F_c^2|)^2/\sum w|F_o^2|^2]^{1/2}$. $w = 1/[\sigma^2(F_o)^2 + 0.0297P^2 + 27.5680P]$, where $P = (F_o^2 + 2F_c^2)/3$.

SMART APEX CCD diffractometer using graphite-monochromated Mo Kα radiation ($\lambda = 0.710\ 73$) at room temperature. The numbers of collected and observed independent [$I > 2\sigma(I)$] reflections are 35 322 and 9840 ($R_{int} = 0.036$) for **1** and 10 213 and 3465 ($R_{int} = 0.029$) for **2**. The data were integrated using the Siemens *SAINT* program.[15] Absorption corrections were applied. The structures were solved by direct methods and refined on F^2 by full-matrix least squares using *SHELXTL*.[16] All non-hydrogen atoms were refined with anisotropic thermal parameters. All of the hydrogen atoms, except those of hydroxy groups and water molecules, were placed in calculated positions. The hydrogen atoms of hydroxy groups and water molecules were located from the difference Fourier maps and refined isotropically with the isotropic vibration parameters related to the non-hydrogen atom to which they are bonded. Crystallographic and refinement details are listed in Table 1, with selected bond lengths and angles in Tables S1 and S2 in the Supporting Information.

Sorption Experiments. In order to determine sorption capacities of **1** (or **2**) toward Fe^{III}, Ca^{II}, Cr^{II}, Mn^{II}, Cu^{II}, Zn^{II}, Cd^{II}, etc., 0.01 g of crystalline **1** (or **2**) was added to 5 mL of a 1 mM metallic chloride aqueous solution and the mixture was allowed to stand for 2 days at room temperature. Then the resultant suspensions were filtered. The initial and final concentrations of all tested elements in solution were measured using a Hitch Z-8000 atom adsorption analyzer. The amounts of adsorbed metal ions were calculated from differences between the concentrations of the metal ions in the filtered solutions and that in the initial solution.

The effect of the reaction time on ferric ion sorption was examined. Five milliliter portions of 1 mM $FeCl_3 \cdot 6H_2O$ solutions were added to 0.01 g of crystalline **1** with a surface area of 2.81 m^2/g or **2** with a surface area of 3.15 m^2/g. The resultant suspensions were filtered at various reaction times. The adsorption amounts of ferric ions were carried out in a Hitch Z-8000 atom adsorption analyzer.

The effect of the initial concentration of Fe^{III} on ferric ion sorption was also examined. Five milliliter portions of $FeCl_3 \cdot 6H_2O$ solutions whose ferric concentrations ranged from 1 to 2.5 mM were added to 0.01 g of crystalline **1** (or **2**) in a glass tube. The tubes were allowed to stand for 2 days at room temperature. Then the resultant suspensions were filtered. The initial and final concentrations of Fe^{III} in solution were measured using a Hitch Z-8000 atom adsorption analyzer. The pH values of the solution before and after each batch experiment were measured.

Results and Discussion

Syntheses. Metal phosphonates are usually prepared by the reaction of a metal salt with a phosphonic acid by a hydrothermal method, by coprecipitation in solution, or by a melt method, of which the hydrothermal method is regarded as the most effective way to produce metal phosphonates.[17] A number of factors involved in the hydrothermal reactions can affect the final products, including the pH, solvent, reaction temperature, and molar ratio of the starting materials, etc. Compounds **1** and **2** have been synthesized by the reaction of $Pb(OAc)_2$ or $ZnCl_2$ with H_8EDTP under hydrothermal conditions in the presence of $N(CH_2CH_3)_3$. The fluoride was added in order to improve the crystallization of the products.[18] Compound **1** is obtained when the molar ratio $Pb(OAc)_2/H_8$EDTP is 3:1 and the pH value of the reactant mixture is adjusted by $N(CH_2CH_3)_3$ to 5.0−6.0.

Single crystals of compound **2** as a monophasic material can be obtained in good yield when the molar ratio of $ZnCl_2/H_8$EDTP is 1:1, the solvent is made of distilled water (5 mL) and C_2H_5OH (5 mL), and the pH value of the reactant mixture is adjusted by $N(CH_2CH_3)_3$ to 5.3. At different molar ratios of the solvent (C_2H_5OH/H_2O) and the starting materials ($ZnCl_2/H_8$EDTP), compound **2** was produced in the form of both crystalline and powder phases.

Structure of 1. As shown in Figures 1 and 2, the structure of compound **1** results from the seven crystallographically different lead atoms that are bridged by two $HEDTP^{7-}$ ligands to yield a three-dimensional microporous framework. The X-ray crystal structure of compound **1** shows a preference of Pb^{II} in a low-coordination geometries with a stereochemically active lone pair.[19] Pb1 is three-coordinated in a slightly distorted tetrahedral environment by binding three oxygen atoms (O5, O10, and O23A) from two $HEDTP^{7-}$ ligands (Figure 1). Pb2, Pb3, and Pb5 are all four-coordinated, and their coordination geometry can be described as a *ψ*-square-pyramidal PbO_4 (or PbO_2N_2) in which the lone pair occupies the fifth coordination site. Pb4 and Pb6 are coordinated by five phosphonate oxygen atoms in a distorted trigonal-bipyramidal geometry with an apex occupied by the lone pair of the Pb^{II} ion. Pb7 is five-coordinated by three phosphonate oxygen atoms (O13, O16, and O22) and two nitrogen atoms (N3 and N4) from the $HEDTP^{7-}$ ligand. The Pb−O bond lengths [2.288(10)−2.671(9) Å] and the Pb−N bond lengths [2.654(9)−2.763(10) Å] may be compared to those in $Pb(H_2L)$ ($H_4L = CH_3N(CH_2PO_3H_2)_2$).[20]

Each $HEDTP^{7-}$ ligand in **1** carries seven negative charges; three phosphonates are deprotonated completely, whereas the

(15) *SAINT*, *Program for Data Extraction and Reduction*, version 6.01; Siemens Analytical X-ray Instruments Inc.: Madison, WI.
(16) Sheldrick, G. M. *SHELXTL, Program for Refinement of Crystal Structures*, version 6.10; Siemens Analytical X-ray Instruments Inc.: Madison, WI.
(17) Wu, J.; Song, Y.-L.; Zhang, E.-P.; Hou, H.-W.; Fan, Y. T.; Zhu, Y. *Chem.—Eur. J.* **2006**, *12*, 5823.
(18) Song, H.-H.; Zheng, L.-M.; Wang, Z.-M.; Yan, C.-H.; Xin, X.-Q. *Inorg. Chem.* **2001**, *40*, 5024.
(19) Claudio, E. S.; Godwin, H. A.; Magyar, J. S. *Prog. Inorg. Chem.* **2003**, *51*, 1.
(20) Mao, J.-G.; Wang, Z.-K.; Clearfield, A. *Inorg. Chem.* **2002**, *41*, 6106.

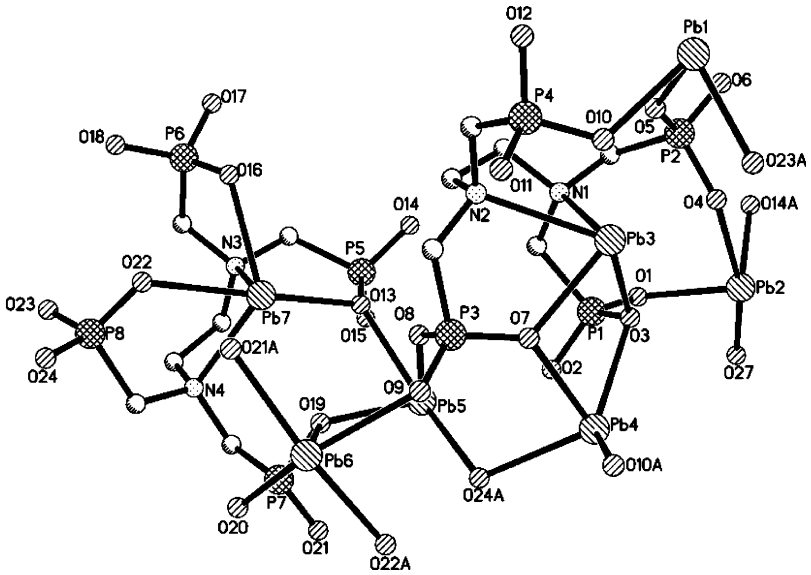

Figure 1. Building unit of structure **1** with an atomic labeling scheme. All lattice water molecules and hydrogen atoms are omitted for clarity.

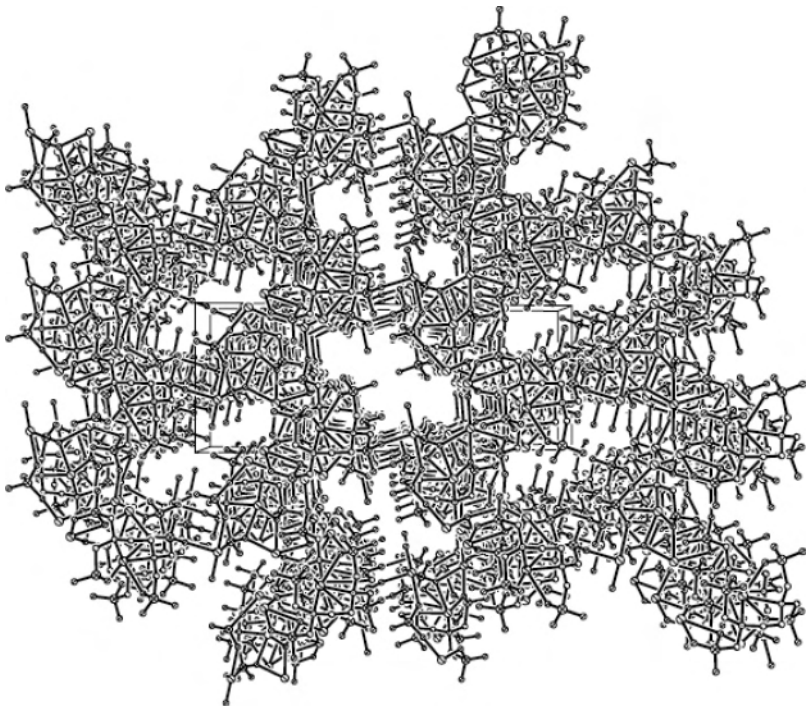

Figure 2. View of the porous three-dimensional network of compound **1** down the *a* axis, emphasizing the tunnel feature. The lattice water molecules and hydrogen atoms are omitted for clarity.

remaining one is ^{1}H-protonated. The hydrogen atoms of the HO_3P groups are attached to the oxygen atoms O11 and O17. The ligands adopt interesting coordination modes in compound **1** (Chart 1). The eight phosphonate groups in two $HEDTP^{7-}$ ligands adopt six types of bonding modes. The phosphonate groups (P2 and P5) adopt a bridging coordination mode, whereas P6 connects with only one metal ion. Using Harris notation,[21] other phosphonate groups can be described as a [3.21] mode, adopted by P1 and P4, a [3.111] mode, adopted by P3, a [3.211] mode, adopted by P7, and a [5.221] mode, adopted by P8.

The interconnection of Pb^{II} ions with phosphonate groups and nitrogen atoms of $HEDTP^{7-}$ results in a three-dimensional microporous network with tunnels along the *a* and *b* axes (Figures 2 and 3). The tunnels along the *a* axis are made of helical chains, which are created by twisted $HEDTP^{7-}$ ligands connected by lead atoms. The cavity of the tunnels is occupied by the seven lattice water molecules in one building unit. As shown in Figure 3, the tunnels along

(21) Harris notation describes the binding mode as [*X*, Y_1, Y_2, Y_3, ... Y_n], where *X* is the overall number of metals bound by the whole ligand and each value of *Y* refers the number of metal atoms attached to the different donor atoms. See: (a) Coxall, R. A.; Harris, S. G.; Henderson, D. K.; Parsons, S.; Tasker, P. A.; Winpenny, R. E. P. *J. Chem. Soc., Dalton Trans.* **2000**, 2349. (b) Brecjin, E. K.; Coxall, R. A.; Parkin, A.; Parsons, S.; Tasker, P. A.; Winpenny, R. E. P. *Angew. Chem., Int. Ed.* **2001**, *40*, 2700.

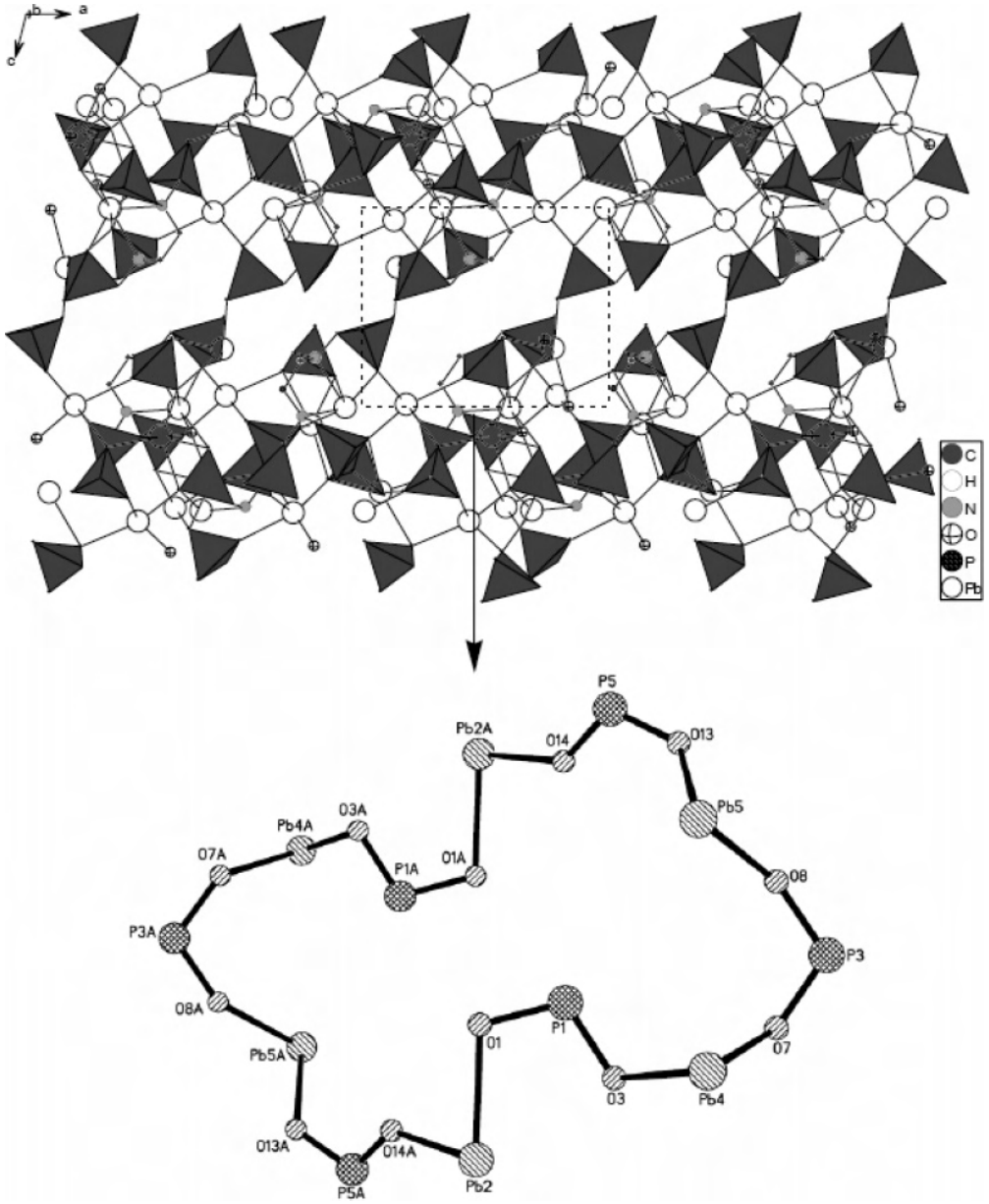

Figure 3. Polyhedral representation of lead phosphonate along the *b* axis. The $C-PO_3$ tetrahedra are shaded in gray. Lead, oxygen, carbon, and nitrogen atoms are represented by open, crossed, gray, and dotted circles, respectively. The lattice water molecules are omitted for clarity.

Chart 1. Coordination Modes of $HEDTP^{7-}$ in Compound **1**

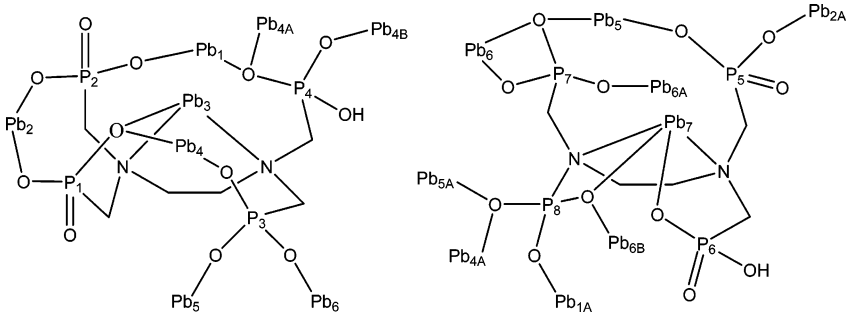

the *b* axis are created by the packing of 24-membered rings, and each ring is formed by six lead atoms and six phosphonate groups. The size of the tunnel is estimated to be about 6.8×10.0 Å^2; thus, it is of the micropore type. It is worth noting that such tunnels can potentially adsorb suitable metal ions or allow for ion exchange between the protons and the metal ions.[22]

Structure of 2. The structure of **2** is different from the microporous structure of **1**. Single-crystal structural determination reveals that **2** crystallizes in space group *Pca*2(1).

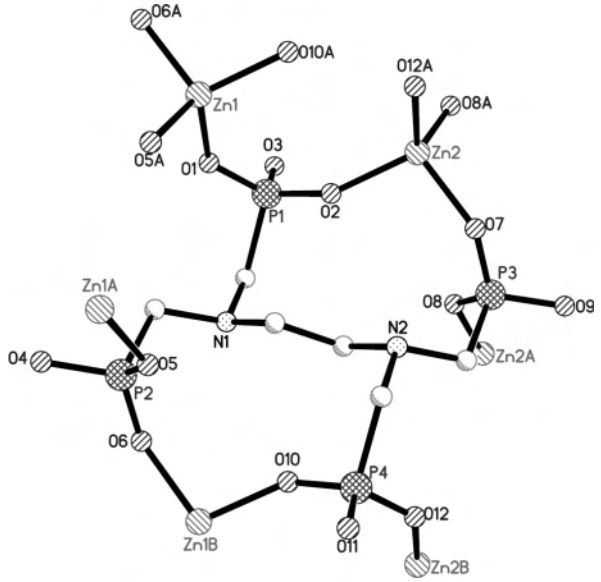

Figure 4. Building unit of structure **2** with an atomic labeling scheme. All lattice water molecules and hydrogen atoms are omitted for clarity.

As shown in Figure 4, the asymmetric structural unit of **2** contains two zinc atoms and one ligand. The ligand carries four negative charges; two phosphonate groups are deprotonated completely, whereas the other two phosphonate groups and the nitrogen atoms remain ^{1}H-protonated, which can be attributed to the zwitterionic behavior of the aminophosphonic acid. The coordination mode of the ligand in **2** differs greatly from that in **1**. The H_4EDTP^{4-} anion bridges with eight Zn^{II} ions and each phosphonate group of H_4EDTP^{4-} in **2** is in the bridging coordination mode, while the nitrogen atoms do not coordinate with any metal ion. Each Zn^{II} ion is coordinated by four phosphonate oxygen atoms in a distorted tetrahedral geometry. The interconnection of Zn^{II} ions by bridging H_4EDTP^{4-} anions resulted in a two-dimensional zinc phosphonate layer with pores along the *c* axis, and the pores are occupied by the lattice water molecules interlinked through hydrogen bonds (Figure 5). This layer also shows a square-wave-like architecture along the *a* axis. As shown in Figure 6, the layers are connected by hydrogen bonds between uncoordinated phosphonate oxygen atoms to form a microporous framework with tunnels. The different structural fashions of **1** and **2** can be attributed to the fact that the coordination number of the Zn^{II} ions in **2** is smaller than that of the Pb^{II} ions in **1**.

The lattice water molecules (O1W and O2W) are not coordinated to the Zn^{II} ions but form strong hydrogen bonds with phosphonate oxygen atoms (O1W···O3 2.915 Å and O2W···O11 2.445 Å) or with nitrogen atoms (N1···O1W 2.691 Å and N2···O2W 2.739 Å) (Table S2 in the Supporting Information).

A major feature of compounds **1** and **2** is their open-framework and microporous structure. This is attributed to the internal pores and tunnels formed by the addition of a polyphosphonic acid spacer to bridge the metal ions. In both **1** and **2**, the dimensions of the tunnels formed inside the

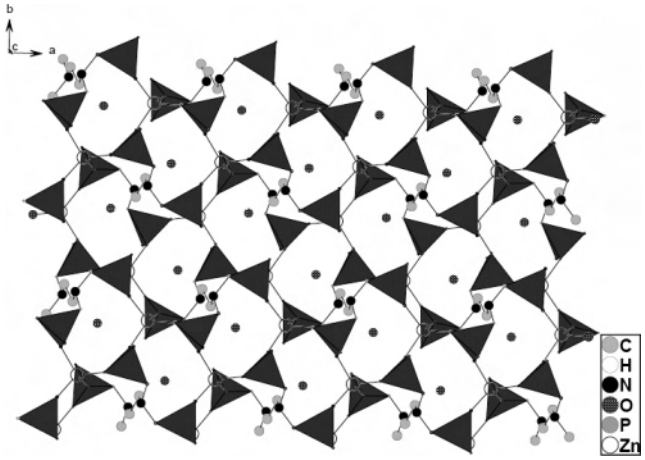

Figure 5. View of one layer of compound **2** along the *c* axis. The phosphonic groups are represented by tetrahedra. Zinc, nitrogen, oxygen, and carbon atoms are shown as open, gray, crossed, and black circles, respectively. All hydrogen atoms are omitted for clarity.

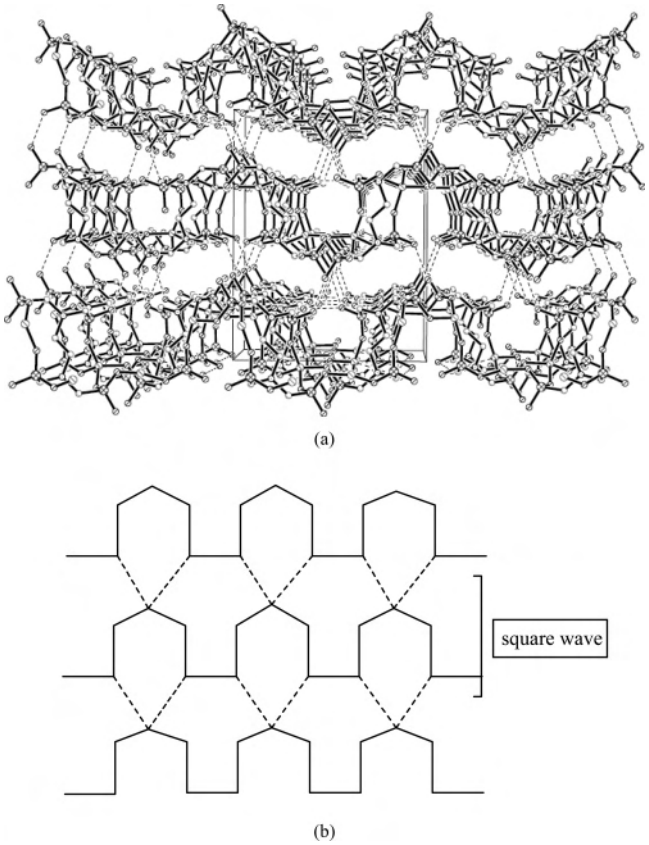

Figure 6. (a) Packing diagram of compound **2** projected down the *a* axis showing the square-wave arrangement of the layers. All of the lattice water molecules and hydrogen atoms are omitted for clarity. (b) Perspective view of the structure of **2** onto the *bc* plane.

structures are determined by the size and geometry of the interlinking organic groups. This feature offers intriguing possibilities to obtaining tailor-made open-framework structures, in which tunnels can be turned for specific purposes by selecting a proper organic group.[13f]

Luminescent Properties. The solid-state luminescent properties of H_8EDTP and compounds **1** and **2** were investigated at room temperature. As shown in Figure 7, the free H_8EDTP ligand shows a strong fluorescent emission

(22) Bao, S.-S.; Chen, G.-S.; Wang, Y.; Li, Y.-Z.; Zheng, L.-M.; Luo, Q.-H. *Inorg. Chem.* **2006**, *45*, 1124.

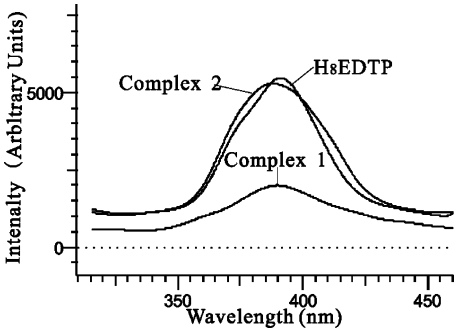

Figure 7. Solid-state emission spectra of H_8EDTP and compounds **1** and **2** at room temperature.

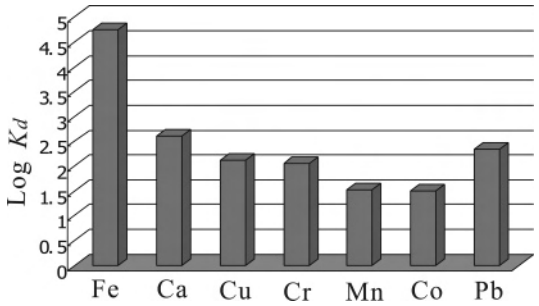

Figure 8. Ion-exchange capability of **1** in an aqueous solution at room temperature.

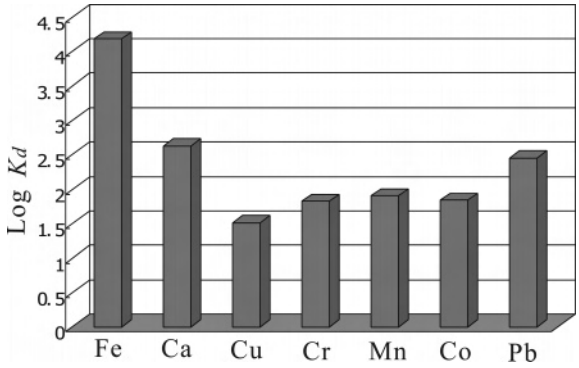

Figure 9. Ion-exchange capability of **2** in an aqueous solution at room temperature.

band at $\lambda_{max} = 391$ nm ($\lambda_{excitation} = 242$ nm); compounds **1** and **2** show broad fluorescent emission bands at $\lambda_{max} = 389$ nm ($\lambda_{excitation} = 245$ nm) and $\lambda_{max} = 387$ nm ($\lambda_{excitation} = 243$ nm), respectively. This demonstrates that the emission spectra of **1** and **2** are neither metal-to-ligand charge transfer nor ligand-to-metal charge transfer in nature but rather are attributed to an intraligand emission state because their fluorescent emission bands are very similar to that of the free ligand.[23] In addition, the fluorescent intensities of the free H_8EDTP ligand and compound **2** are more than 2 times that of compound **1**. This can be attributed to the coordination of nitrogen atoms of the H_8EDTP ligand to lead ions in **1**, which obviously decreases the rigidity of compound **1** and increases the loss of energy via radiationless decay of the intraligand emission excited state.

Ion Sorption and Exchange. Compared with the traditional ion sorption and exchange materials, metal tetraphosphonates have many advantages: (1) They always have porosity with large surface area and tunnels, which facilitate the movement of the adsorbed metal ions inside the compounds without steric impediments and promise rapid uptake of them. (2) The negative charge of metal tetraphosphonates is concentrated on the proton-bearing oxygens, which spread over in the tunnels and show strong attraction to cations by electrostatic bonding. (3) More importantly, we can modify and tailor the dimensions of the tunnels inside these structures to suit certain ions by the right choice of the interlinking organic group. (4) They possess an effective ion-exchange capacity and are more thermally stable than the organic-based exchangers. Compounds **1** and **2** with open-framework and microporous structures were synthesized with the use of tetraphosphonic acid, H_8EDTP, having potential applications in selective ion sorption and exchange.

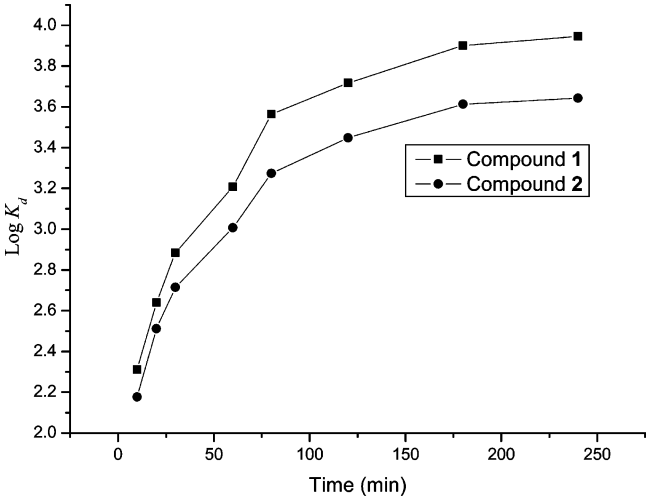

Figure 10. Relationship between the ion sorption amount of the ferric ion as log K_d and the reaction time for compounds **1** and **2**.

To assess their metal ion sorption and exchange capacities, 0.01 g of crystalline **1** (or **2**) was added to 5 mL of a 1 mM metallic chloride aqueous solution and the mixture was allowed to stand for 2 days at room temperature. The initial and final concentrations of all tested elements in solution were measured using a Hitch Z-8000 atom adsorption analyzer. The distribution coefficient (K_d) was determined according to the following equation:[11b]

$$K_d = \frac{C_0 - C_f}{C_f}\frac{V}{m_s}$$

where C_0 and C_f are the initial and final metal ion concentrations in solution (mM), V is the solution volume (mL), and m_s is the mass of the sorbent (g).

As shown in Figures 8 and 9, compounds **1** and **2** exhibit high ion sorption capacities for millimolar concentrations of Fe^{III}, with log $K_{d,Fe^{III}}$ values of 4.75 for **1** and 4.18 for **2**. Specifically, compound **1** adsorbed nearly 100% of Fe^{III} ($C_f < 0.01$ mM), and compound **2** adsorbed 96.8% of Fe^{III} ($C_f = 0.03$ mM). They were also found to extract Fe^{III} selectively over Ca^{II}, Cu^{II}, Cr^{II}, Mn^{II}, Pb^{II}, and Co^{II}, with $K_{d,Fe^{III}}/K_{d,M^{II}}$ values for compound **1** of 137 (for Ca), 411 (for Cu), 498 (for Cr), 1689 (for Mn), 106 (for Pb), and 1715 (for Co)

(23) Song, J.-L.; Zhao, H.-H.; Mao, J.-G.; Dunbar, K. R. *Chem. Mater.* **2004**, *16*, 1884.

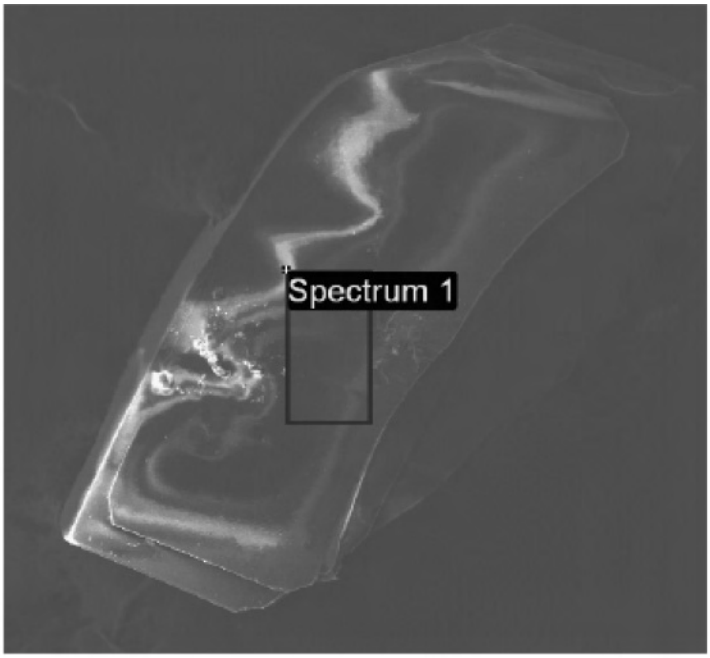

(a)

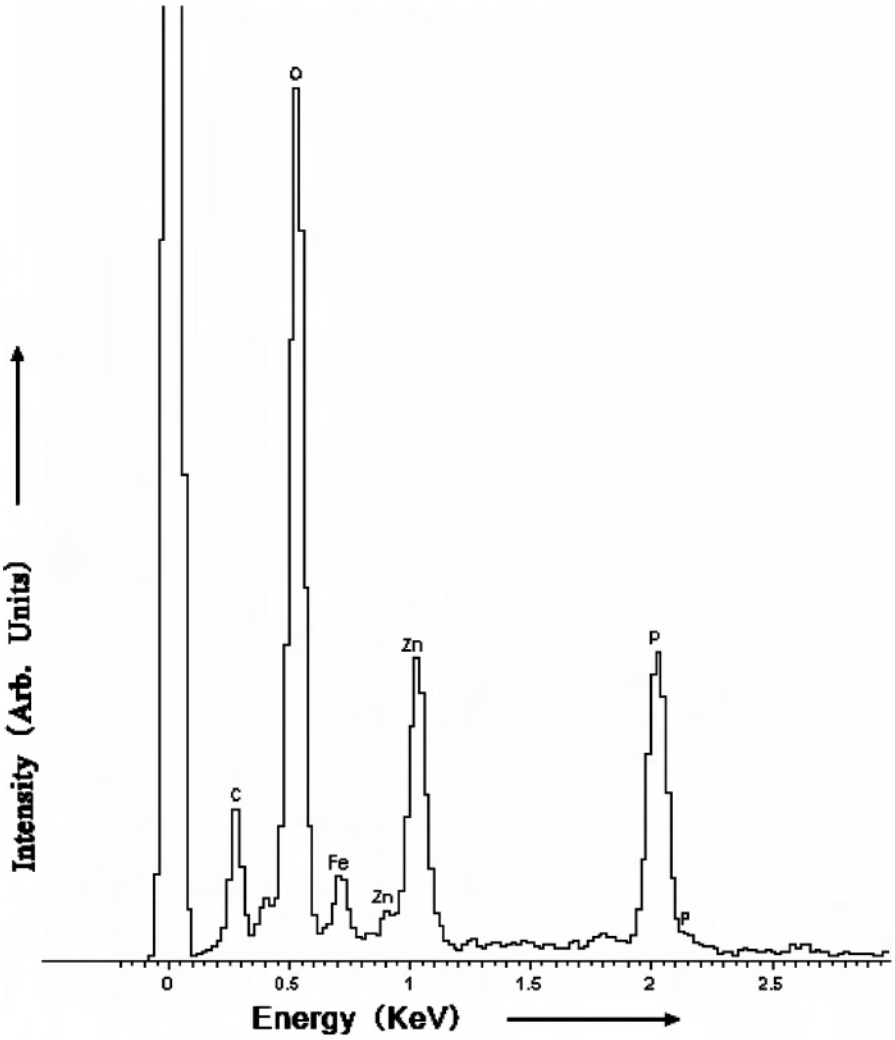

(b)

Figure 11. SEM (a) and EDS (b) for the surface of **2**.

Table 2. Ferric Ion Sorption Capacities of Compounds **1** and **2** with Different Initial Concentrations of Fe^{III}

		compound **1**			compound **2**		
[Fe] concn (mM)	pH	removal (%)	pH value after sorption	log K_d	removal (%)	pH value after sorption	log K_d
1	2.43	100	2.84	4.75	96.8	2.89	4.18
1.5	2.18	92.2	2.41	3.77	86.3	2.44	3.50
2	2.09	79.4	2.27	3.29	72.1	2.33	3.22
2.5	1.98	69.0	2.18	3.04	69.3	2.15	3.06

and values for compound **2** of 36 (for Ca), 465 (for Cu), 231 (for Cr), 189 (for Mn), 54 (for Pb), and 222 (for Co). Meanwhile, Zn^{II}, Cd^{II}, Ni^{II}, Na^{I}, and K^{I} were not adsorbed to any appreciable extent for both compounds **1** and **2**. This may ascribe to the facts that the sorbing sites of both the crystalline sorbents are more accessible to ferric ions and the frameworks have a strong affinity for ferric ions.

The relationship between the amounts of Fe^{III} adsorbed on both compounds and the reaction time is shown in Figure 10. As can be seen, the amount of adsorbed Fe^{III} increased with the reaction time within 4 h. After 4 h, the amount of Fe^{III} ions in solution became scanty and the colors of the solution were shaded from orange to colorless. This is quite different from those of resins and zeolites, in which the adsorbed ions always achieve equilibrium within 1 h.[24] The results indicated that the sorption takes place in the crystalline metal phosphonate by diffusion of ions from the outer surface inward with an advancing phase boundary. Thus, it is easy to comprehend that the facile ion sorption may occur in structures with tunnels, interconnected cages, or layers of sufficient dimensions to allow ion transport.

In order to give a quantitative description of the Fe^{III} distributions in the sorbents, a single crystal of **2** was added to a 1 mM $FeCl_3 \cdot 6H_2O$ solution and the mixture was allowed to stand for 2 days at room temperature. Then the EDS measurements on this crystal were carried out. Figure 11 shows the SEM and EDS results of the single-crystal surface. The detected atom ratios for carbon, oxygen, phosphorus, iron, and zinc were 20.40%, 51.46%, 9.65%, 1.84%, and 16.67%, respectively. After cutting this crystal, we measured the Fe^{III} distributions inside the crystal (Figure 12). We can see that, at the peripheral of the crystal (spectrum 2), the detected atom ratios for carbon, oxygen, phosphorus, iron, and zinc were 39.33%, 40.23%, 7.19%, 1.00%, and 12.25%, respectively, and that on the middle of the crystal (spectrum 1), they were 22.79%, 54.21%, 8.16%, 0.38%, and 14.46%, correspondingly. Obviously, the ion adsorption reactions for Fe^{III} took place mainly on the surface of the crystalline materials, and only a small quantity of Fe^{III} could be adsorbed into the interior of the single crystal by coordination, electrostatic bonding, and ion exchange. Furthermore, there is a diminishing concentration gradient of Fe^{III} from the crystal surface to the interior.

The effect of the initial concentration of Fe^{III} on ion sorption was examined. As shown in Table 2, an increase in the sorption capacity and a decrease of the uptake percent with an increase of the initial concentration were characteristic of the sorbents **1** and **2** in adsorption of the ferric ion. In addition, the solution of $FeCl_3 \cdot 6H_2O$ is acidic owing to their hydrolysis (pH about 2). An increase in the pH of the solution after adsorption may arise from the shift of hydrolysis equilibration with the loss of ferric ions in the solution, though some protons are exchanged into the solution by Fe^{III}. When the initial concentration of Fe^{III} is 1 mM, the results of analysis showed that compounds **1** and **2** picked up 0.50 and 0.48 mmol/g of ferric ions from the solution, respectively. The initial pH of the solution is 2.43 and changes to 2.84 for **1** and 2.89 for **2** after adsorption. Protons were released to the solution after ion sorption, as evidenced by the low pH values although almost all ferric ions were adsorbed. The amount of adsorbed ferric ions of compound **1** is more than the value of its exchange capacity for Fe^{III} by theory calculation. This demonstrates that compound **1** has other chemical and physical affinities for ferric ions besides ion exchange. In addition, after adsorption both compounds changed from white to yellow. The atom adsorption measurements on the final products after adsorption of **1** and **2** revealed that the molar ratios of the metal ions are 1:0.16 for Pb/Fe and 1:0.08 for Zn/Fe, respectively. The results are in accordance with those calculated theoretically from the differences between the concentrations of the ferric ions before and after the ion adsorption. The elemental analyses on the products after adsorption show that the contents of C, H, and N in **1** changed into C (5.74), H (0.89), and N (2.14) and in **2** they changed into C (11.65), H (3.44), and N (4.11). The XRD patterns of **1** and **2** showed that there were no significant changes in the reflex positions before and after sorption, some changes took place in the reflex intensity before and after sorption (Figures S1 and S2 in the Supporting Information). This may be due to the facts that the ion adsorption reactions for Fe^{III} took place mainly on the surface of the sorbent and only a small quantity of Fe^{III} could be adsorbed into the interior.

The interesting ferric ion sorption properties of **1** and **2** are closely associated with their particular structural characteristics. The structure of compound **1** shows a three-dimensional microporous network with tunnels along the *a* and *b* axes, which will facilitate the movement of the Fe^{III} ions through the tunnel network and promise rapid uptake of this ions. The uncoordinated phosphonates oxygen atoms spread over these tunnels and show a strong affinity to Fe^{III} by electrostatic attraction. Compound **2** features a layered structure with pores along the *c* axis and a square-wave-like architecture along the *a* axis. The layers are held together by hydrogen bonds, and the interlayer distance is large enough for ingoing ions to diffuse into the interlamellar spacing. The ingoing ferric ions can lie between the planes and serve to bind the layers together by electrostatic attractions. Meanwhile, the uncoordinated phosphonate oxygen atoms and amino groups have the ability to bind the ingoing ferric ions.

(24) (a) Trochimczuk, A. W. *Eur. Polym. J.* **1998**, *34*, 1047. (b) Shaw, M. J.; Nesterenko, P. N.; Dicinoski, G. W.; Haddad, P. R. *J. Chromatogr. A* **2003**, *997*, 3. (c) Watanabe, Y.; Yamada, H.; Tanaka, J.; Komatsu, Y.; Moriyoshi, Y. *Sep. Sci. Technol.* **2004**, *39*, 2091.

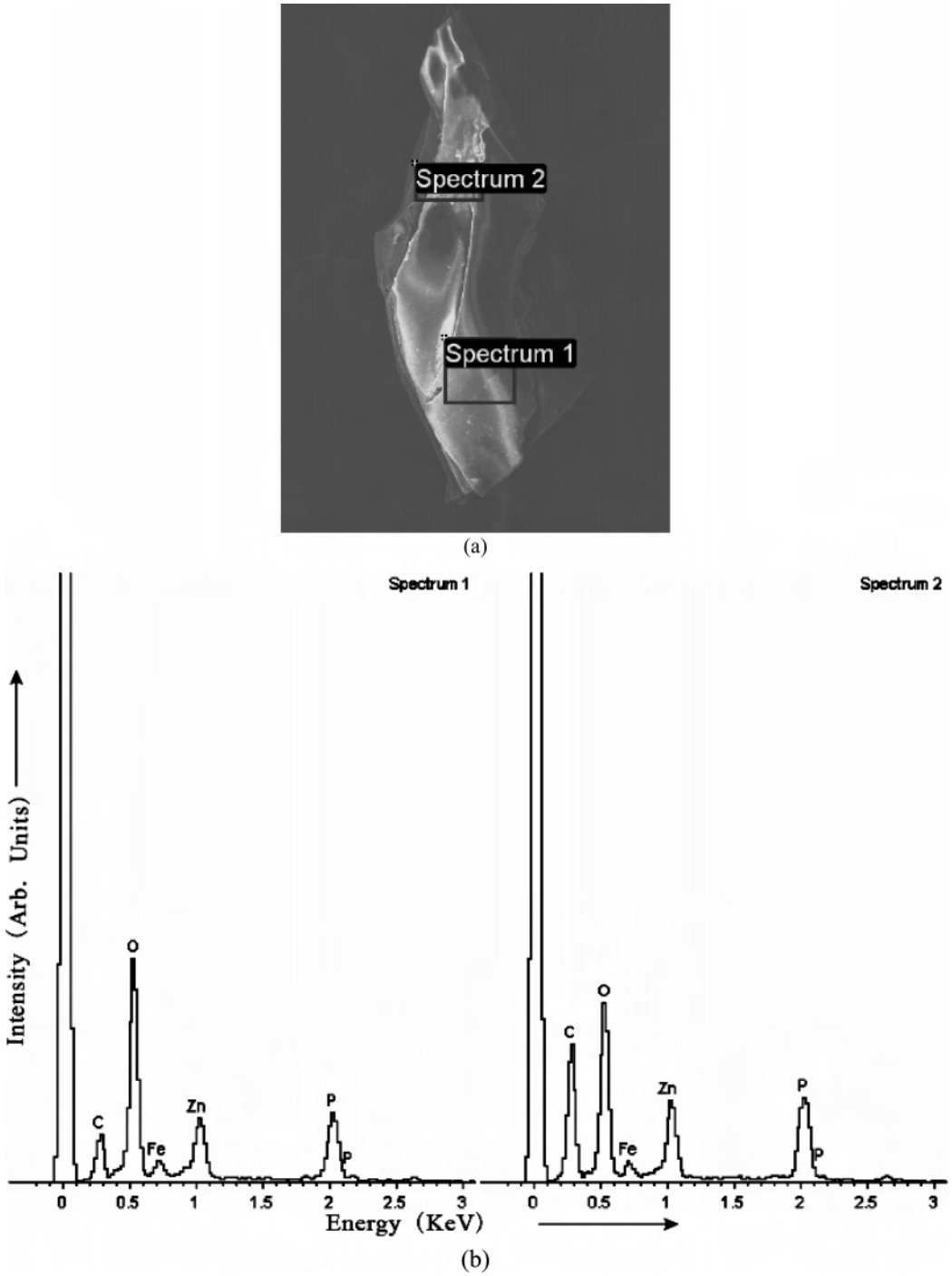

Figure 12. SEM (a) and EDS (b) for the interior of **2** after a single crystal is cut.

Conclusion

The reaction of H_8EDTP with lead acetate or zinc chloride under hydrothermal conditions has resulted in two novel open-framework and microporous materials, $\{[Pb_7(HEDTP)_2(H_2O)]\cdot 7H_2O\}_n$ (**1**) and $\{[Zn_2(H_4EDTP)]\cdot 2H_2O\}_n$ (**2**), showing unique tunnel structures and exhibiting a high affinity for ferric ions. They were also found to possess a high selectivity for ferric ions, which may arise not only from ion exchange but also from the strong coordination bonding and electrostatic attractions to ferric ions with phosphonate groups. The experimental results indicated that the ion adsorption reactions for Fe^{III} took place mainly on the surface of the crystalline materials and a small quantity of Fe^{III} could be adsorbed into the interior of the sorbents. Thus, compounds **1** and **2** seem to be promising materials for the selective adsorption and exchange of ferric ions from aqueous solutions.

In addition, metal tetraphosphonates can be considered as a new class of excellent cation sorption and exchange materials because of their insolubility, thermal stabilization, and tailor-made cavities for specific cations. The results set the stage for using analogous metal tetraphosphonate for selective adsorption of other cations, eluating aspects of selectivity and determining the sorption mechanism involved.

Acknowledgment. We thank the National Natural Science Foundation of China (Grants 20671082 and 20371042) for support.

Supporting Information Available: X-ray crystallographic files in CIF format for the two compounds, selected bond lengths and angles for compounds **1** and **2**, XRD patterns for compound **1** obtained with the use of NaOH or $NH_3 \cdot H_2O$, and XRD patterns of the products after ion exchange with Fe(III). This material is available free of charge via the Internet at http://pubs.acs.org.

IC062014X